Unsupervised Selection of Color Factor Weight and Segmentation Scale Parameter for Successful Segmentation of Urban Land Use/Land Cover.

[1]Guy Blanchard Ikokou, [2]Kate Miranda Malale

[1,2,] Tshwane University of Technology, Pretoria, South Africa

Keywords: Remote sensing, image segmentation, scale parameter, color factor weight, object-based Image Analysis.

Abstract:

Image segmentation is a crucial step in object-based image analysis of urban remote sensing data. Its primary goal is to divide a digital image into meaningful objects that are internally homogeneous and clearly distinguishable from neighboring segments. While the segmentation scale parameter helps limit the size of these image segments, it alone cannot guarantee optimal intra-segment homogeneity or inter-segment separability. Many existing segmentation quality assessment methods rely on spatial autocorrelation measures, which often lead to irregular variations in the global objective function. As a result, segments representing spectrally distinct but spatially large objects may be incorrectly merged during the final stages of segmentation, leading to significant over- and under-segmentation errors. This paper presented an unsupervised hybrid segmentation evaluation strategy that combines the Moran's index and the image standard deviation measures. The proposed segmentation evaluation strategy was tested on a color aerial image of the Cape Town metropolitan area. Experimental results show that the proposed approach successfully identified optimal combinations of scale parameters and color factor weights that minimize over- and under-segmentation of the image. The approach achieved very promising over- and under-segmentation (OS and US), as well as area fit index (AFI) error magnitudes, in comparison to some of the existing state-of-the-art approaches available in the literature. It was also found that associating small weights of color factor with medium-range scale parameters resulted in optimal segmentation outcomes, while larger segmentation scale parameters required large weights of the color factor to produce meaningful segmentation outcomes. Furthermore, it was uncovered that the spatial autocorrelation curve achieved stability at optimal segmentation parameters and a near horizontal fluctuation shape, describing a drop of image variance to values very close to zero at optimal segmentation parameters.

1. Introduction

Object-oriented image analysis holds the advantage of classifying a digital image based on the spectral, spatial, and contextual attributes of a group of homogeneous pixels, in contrast to pixel-based image analysis (Ozturk and Colkesen, 2024). The successful grouping of homogeneous pixels as "objects" generally depends on the inter-pixel spatial autocorrelation and intra-pixel homogeneity measures, which, in turn, depend on a set of user-defined parameters that include the segmentation scale parameter, the shape factor, and the color factor (Kavzoglu and Yildiz, 2014). The segmentation scale parameter, while useful for limiting the size of image segments, is not sufficient on its own to guarantee optimal intra-segment homogeneity or inter-segment separability (Ez-zahouani et al., 2023). Achieving optimal intra-segment homogeneity and inter-segment heterogeneity requires some numerical balance between the segmentation scale parameter and the weights assigned to the shape or color factors, respectively (Ikokou and Smit, 2021). An unbalanced combination of the segmentation scale parameter and the weights assigned to the shape or color factor can result in high intra-segment heterogeneity (Dracut et al., 2014). The selection of an optimal combination between the segmentation scale parameter and the shape factor has attracted high attention among the remote sensing community for the past decade (Johnson et al., 2015; Zhu et al., 2016; Grippa et al., 2017; El-Nagger, 2018; Yang et al., 2019; Norman et al., 2019; Lu et al., 2021; Cai et al., 2022; Ez-Zahouani et al., 2023**;** Johnson et al., 2024). In contrast, studies on the correlation between the segmentation scale parameter and the weights assigned to the color factor are lacking among the current remote sensing literature (Ikokou and Malale, 2024). Finding an image variance and spatial dependence balance between the scale parameter and the weight assigned to the color factor has been described as difficult since the selection strategy is generally based on trial-and-error visual assessments (Blaschke, 2010**).** Several unsupervised strategies for the selection of optimal segmentation parameters have been described in the remote sensing literature (Grybas et al., 2017; Georganos et al., 2018; Wang et al., 2019; Tonbul et al., 2020). These approaches mostly rely on metrics such as the Moran spatial autocorrelation index and the image weighted variance. However, the performance of the Moran index as a spatial autocorrelation measure was reported to be poor when used for complex landscapes such as urban areas. When estimating the inter-segment spatial autocorrelation measure, the Moran index generally does not make any distinctions between adjacent and non-adjacent homogeneous segments, leading to a false spatial autocorrelation measure (Hu et al., 2018). In addition, the weighted image variance cannot model irregular image variances that are inherent to remote sensing images covering urban areas (Chen et al., (2018). This study presents a novel spatial correlation framework designed to optimize the combination of the segmentation scale parameter and the associated numerical weight of the color factor.

2. Methodology

2.1. Feature Selection and Extraction

In this study, the multiresolution segmentation algorithm available in eCognition software was applied to segment the aerial photograph into meaningful image objects. A weight of one was given to each of the aerial image’s four spectral bands in order to establish an equal spectral contribution of all the bands into the segmentation process. The shape smoothness of image segments was voluntarily calibrated at 0.5 as a balanced threshold. Table 1 presents the various scale parameters and associated color factor weights used in the initial segmentations that produced spatial and spectral attributes of image segments.

Color factor thresholds	**0.1**	**0.2**	**0.3**	**0.4**	**0.5**	**0.6**	**0.7**	**0.8**	**0.9**
Scale parameters	50	50	50	50	50	50	50	50	50
	70	70	70	70	70	70	70	70	70
	90	90	90	90	90	90	90	90	90
	110	110	110	110	110	110	110	110	110
	130	130	130	130	130	130	130	130	130
	150	150	150	150	150	150	150	150	150

Table 1. Presents the parameters used for the initial segmentation phase in order to derive the segment brightness and area measures

From the resulting segments, 801 unique spectral signatures and area measures associated with individual image segments were collected. Table 2 presents a subset of residential and nonresidential building sample sizes as well as the spectral brightness associated with each sample segment measured from twelve segmentation scale parameters.

Residential/nonresidential buildings’ spectral brightness measures	Segment area measures (square pixel)	Residential/nonresidential buildings’ spectral brightness measures	Segment area measures (square pixel)
143.43	135.4	45.68	471
14.46	227.97	17.68	262
14.83	233.63	61.44	438
176.79	197.15	51.96	519
36.14	193.5	116.96	234
229.31	229.54	132.71	252
57.12	209.69	188.36	181
23.61	159.22	252.29	172
152.24	226.01	244.32	614
45.06	200.59	163.45	118
20.83	176.32	141.67	268
56.63	106.67	222.35	198
103.8	434	476	366
228	827	214.53	456
141.75	510	199.01	868
80.72	275	216.27	536
28.31	300	182.864	289
78.59	877	144.88	315
32.32	587	243.93	921
205.44	523	249.98	616
210.95	557	170.37	549
207.05	254	241.83	585
245.61	261	214.63	246
224.37	200	193.95	269

Table 2. A sample of collected segments brightness measures and their associated image area sizes in square pixel

2.2. Calibrating color factor weights per segmentation scale parameter

Due to the limitation of the weighted image variance to handle spectral irregularities between image segments, we replaced the measure by the standard deviation model. High values of this measure are associated with segments with low internal homogeneity and vice versa. The formulation of this model adopted in this study is given as follows:

$$K = \frac{\sum_{i=1}^{n} \sqrt{\left(\lambda_i - \bar{\lambda}\right)^2}}{\sum_{i=1}^{n} \rho_i} \tag{1}$$

The quantity in the denominator describes the sum of the area measures associated with all segments at individual segmentation levels. The measure λ_i is the segment grey level recorded measure, while the quantity $\bar{\lambda}$ is the average grey level associated with the segmentation level. To estimate the spatial dependency between adjacent image segments, we proposed a model derived from the correlation coefficient and formulated it as follows:

$$S_g = \frac{\left(\sum_{q=1}^{p}\left(z_i - \bar{z}\right)^2 \left(\sum_{q \neq r} \sum S_{ij}\right)\right) \sum_{i=1}^{n} c_i \sqrt{\left(\lambda_i - \bar{\lambda}\right)^2} + p \sum_{q=1}^{p} \sum_{r=1}^{p} S_{ij}\left(z_i - \bar{z}\right)\left(z_i - \bar{z}\right)\left(J\right)}{\left(J\right) \sum_{q=1}^{p}\left(z_i - \bar{z}\right)^2 \left(\sum_{q \neq r} \sum S_{ij}\right)} \tag{2}$$

Where p represents the total number of objects, while z_i is the spectral value of a segment i and $\bar{z}$ denotes the mean spectral values of objects across the entire image. The variable S_{ij} serves as a spatial proximity indicator between objects i and j, taking a binary value: $S_{ij} = 1$ if objects i and j are adjacent and share a common boundary, and $S_{ij} = 0$ if they are not spatially connected. The measures λ_i and $\bar{\lambda}$ are defined according to the model presented in Equation (1). Higher values of the index S_g correspond to lower inter-object heterogeneity, while lower values indicate greater dissimilarity between objects. To achieve good segmentation results, we need high intra-segment homogeneity through the model in **(1)** and high inter-segment homogeneity through the model in **(2).** These two needed attributes were combined in a global score function defined as follows:

$$G = \frac{\left(S_g\right)_{norm} - K_{norm}}{\left(S_g\right)_{norm} + K_{borm}} \tag{3}$$

As the value of the index approaches one, the image segments become more internally homogeneous and more distinct from their neighboring segments at a given segmentation level (Ikokou and Malale, 2024). Based on the calculated image variance and corresponding spatial dependence measures, normalized values were derived. Tables 3 and 4 present the estimated normalized image variance and spatial dependence metrics, respectively.

Numerical color factor weight	**Normalized-image-variance at segmentation scale parameter of 50**	**Normalized-image-variance at segmentation scale parameter of 70**	**Normalized-image-variance at segmentation scale parameter of 90**
0.2	0,106	0,053	0,849
0.3	0,114	0,389	0,317
0.4	0,141	0,401	0.451
0.5	0,048	0,434	0.10
0.6	0.002	0,135	0,356
0.7	0.087	0.568	0,072
0.8	0,188	0.213	0,148
0.9	0,061	0,145	0,130
Numerical color factor weight	Normalized-image-variance at segmentation scale parameter of 110	Normalized-image-variance at segmentation scale parameter of 130	Normalized-image-variance at segmentation scale parameter of 150
0.2	0.237	0,067	0,547
0.3	0,157	0,892	0.792
0.4	0,260	0.421	0,208
0.5	0.642	0,559	0,109
0.6	0,145	0,488	0,348
0.7	0,161	0,501	0,485
0.8	0,009	0.064	0.389
0.9	0,032	0,041	0,554

Table 3. Optimized image variance measures per segmentation levels at six segmentation scale parameters.

https://doi.org/10.5194/isprs-archives-XLVIII-G-2025-679-2025 | © Author(s) 2025. CC BY 4.0 License.

Numerical color factor weight	Normalized-spatial dependence at scale parameter of 50	Normalized-spatial dependence at scale parameter of 70	Normalized-spatial dependence at scale parameter of 90
0.2	0.101	0.107	0.065
0.3	0.423	0.113	0.432
0.4	0.435	0.140	0.368
0.5	0.466	0.049	0.818
0.6	0.184	0.948	0.268
0.7	0.900	0.128	0.315
0.8	0.01	0.187	0.184
0.9	0.193	0.059	0.250
Numerical color factor weight	Normalized-spatial dependence at scale parameter 110	Normalized-spatial dependence at scale parameter 130	Normalized-spatial dependence at scale parameter 150
0.2	0.697	0.095	0.061
0.3	0.355	0.259	0.101
0.4	0.060	0.002	0.706
0.5	0.852	0.257	0.898
0.6	0.353	0.111	0.318
0.7	0.069	0.228	0.438
0.8	0.148	0.679	0.162
0.9	0.130	0.879	0.261

Table 4. Optimized spatial autocorrelation of the image evaluated across segmentation levels at six different scale parameters.

2.3. Segmentation parameter combination optimization

From tables 3 and 4, we combined the lowest image variance with the highest segments ‘spatial dependence measures and then computed the global index measure. Table 5 presents the achieved computation results. The values in the fourth column of the table were computed using equation 3.

Scale Parameter	**Lowest values of the normalized standard deviation in the image**	**Maximum normalized spatial dependence measures**	**Global Index measures**
50	0.002	0.900	0.996
70	0.053	0.948	0.894
90	0.072	0.818	0.838
110	0.009	0.852	0.979
130	0.041	0.879	0.911
150	0.109	0.898	0.784

Table 5. Computed optimal heterogeneity function values for each scale parameter

Since most global score estimates are closely clustered, normalizing these values allows for better differentiation. Table 6 presents the normalized global scores corresponding to each segmentation scale parameter. At a scale parameter of 50, pairing with a color factor weight of 0.6 yielded the lowest image variance, whereas the highest inter-segment spatial autocorrelation (99.6%) was achieved with a color weight of 0.7, producing segments that are both internally homogeneous and well-separated from their neighbors. For a scale parameter of 70, the lowest image variance occurred at a color weight of 0.2, while the highest inter-segment heterogeneity (89.4%) was observed at a color weight of 0.6, indicating strong segment distinctness and internal consistency. At scale 90, both the lowest image variance and highest inter-segment heterogeneity (approximately 84%) were attained with a color weight of 0.5. Similarly, a color weight of 0.8 combined with scale 110 resulted in the lowest image variance, whereas a color weight of 0.5 at this scale produced the highest inter-segment heterogeneity, yielding segments with 98% internal homogeneity and distinctness. At scale 130, the lowest image variance corresponded to a color weight of 0.8, and the highest spatial autocorrelation (about 91%) was achieved with a color weight of 0.9. Lastly, the combination of scale 150 and color weight 0.5 produced both the lowest image variance and highest spatial autocorrelation, with segments attaining approximately 78% internal homogeneity and separability.

The smallest magnitude of the normalized global score was achieved with the scale parameter of 150, which is followed by that achieved at scale parameter 90. The third lowest magnitude of the index was achieved at scale parameter 70, which is followed by that achieved at scale parameter 130 as presented in table 6. The scale parameters 50 and 110 produced the highest magnitudes

https://doi.org/10.5194/isprs-archives-XLVIII-G-2025-679-2025 | © Author(s) 2025. CC BY 4.0 License.

of the global score index and are suggested to be suitable for the segmentation of the selected urban scene.

Scale Parameter	Lowest Normalized Image standard deviation Measures	Largest Normalized Spatial dependence measures	Normalized Global Index measures
50	0.002	0.900	1
70	0.053	0.187	0.519
90	0.072	0.818	0.255
110	0.009	0.852	0.919
130	0.041	0.879	0.599
150	0.109	0.898	0

Table 6. Computed normalized global score index values per segmentation scale parameter.

3. Experimental results

From the last column of table 6, we refined and the identified the best segmentation parameter combinations by producing a global score curve in MS Excel. Figure 1 presents the identified optimal parameter combinations. The scale parameters of 50 and 110 are suggested to produce image segments with the best internal homogeneity as well as the best inter-segment heterogeneity measures. Since the values of the global score are an indication of optimal parameter combination, it is expected that peak points are descriptive of the suitable scale parameter-color factor combination that would accurately segment the urban scene under consideration.

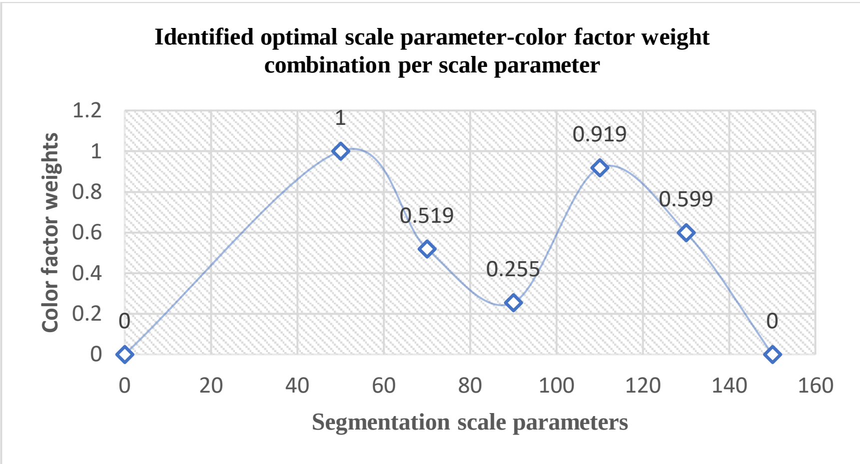

Figure 1: Fluctuations of the segment quality global score index per segmentation parameter and color factor weight

From figure 1, it is suggested that our urban scene only needs two segmentation levels to describe the medium-sized and large buildings characterizing the scene as illustrated in Figures 2 and 3.

Figure 2. (A) Over segmentation of medium sized buildings at scale parameter of 35 and (B) optimal segmentation of medium sized building units at scale parameter of 50

Figure 3 illustrates the segmentation results of large building units at scale parameters 90 (A) and 110 (B). As previously noted, the segments produced at scale 90 exhibit internal instability, particularly in terms of brightness, which also extends to surrounding tree cover and green areas adjacent to the buildings. In contrast, segmentation at scale 110 effectively reduces internal variance by merging smaller segments into larger, more coherent ones. This results in a more accurate reconstruction of the outlines of large building units and nearby tree patches, demonstrating improved segmentation performance.

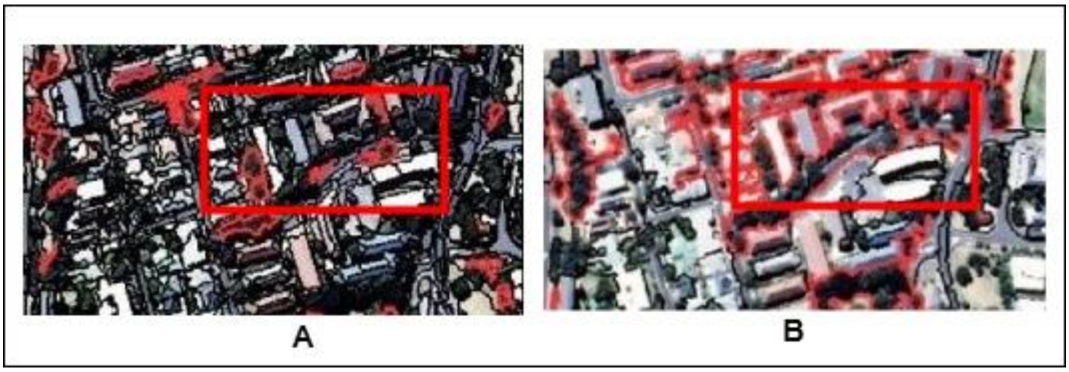

Figure 3. (A) Over segmentation of large building units at scale parameter of (90) and (B) optimal segmentation of large building units

4. Accuracy Assessment

Five metrics were considered in this study to evaluate our segmentation performance. These include the quality rate (QR), the area fit index (AFI), the over and under segmentations (OS),and (US) as well as the root mean square (RMS) measure. To compute these five assessment measures, we manually digitized medium-sized and large buildings using ArcGIS version 10.8. Individual segment area measures were collected in order to be used concurrently with associated segment areas. A total of 101 sample segments were carefully considered throughout the urban scene. Table 7 shows a subset of the computed evaluation matrix.

segments	Digitized area	Segmented areas	QR	AFI	OS	US	RMS
1	143.43	135.4	0.028799	0.028799	0.055985	0.059306	0.05767
2	14.46	14.7	0.00823	-0.00823	0.016598	0.016327	0.016463
3	14.83	13.63	0.042164	0.042164	0.080917	0.088041	0.084554
4	17.68	19.71	0.054293	-0.05429	0.114819	0.102993	0.109067
5	36.14	35.91	0.003192	0.003192	0.006364	0.006405	0.006385

6	29.31	29.94	0.010633	-0.01063	0.021494	0.021042	0.021269
7	57.12	59.69	0.022002	-0.022	0.044993	0.043056	0.044035
8	23.61	22.59	0.022078	0.022078	0.043202	0.045153	0.044188
9	25.24	26.01	0.015024	-0.01502	0.030507	0.029604	0.030059
10	20.83	26.32	0.116437	-0.11644	0.263562	0.208587	0.237669

Table 7. A sample of estimated segmentation assessment metrics to evaluated our proposed strategy

An analysis of the quality rate column indicates that the proposed segmentation parameter selection method successfully generated a majority of image segments whose sizes closely align with the actual outlines of real-world objects. The approach successfully minimized over-segmentation of the urban scene, as confirmed by the area fit index and the under-segmentation columns. It has been reported in the literature that under-segmentation is preferable in object-based image analysis to over-segmentation.
From the second column of Table 8, it can be observed that the approach presented in Norman et al. (2020) did not produce very good quality segments characterized by the large estimate of the quality rate parameter. In contrast, our parameter selection strategy produced the best segment quality described by the lowest estimate of the quality rate index. This suggests that the overall under-segmentation error identified in table 7 is very negligible. The strategy proposed in Norman et al. (2020) achieved the lowest but positive area fit index measure. This suggests that the majority of segments produced by the parameters selected through this strategy were highly subjected to over-segmentation. Our approach achieved the lowest negative estimate of the parameter, confirming early observation that most of the segmented objects were subjected to minimal under-segmentation. The parameter selection strategy proposed in Norman et al. (2020) produced the lowest under-segmentation index; this indicates that most segments were subjected to over segmentation. However, a look at the quality rate measure suggests that the magnitudes of individual under-segmented errors are actually very large, compared to those achieved through our selection strategy. The over segmentation metric column suggests that the newly proposed parameter selection strategy successfully minimized the individual under-segmentation errors throughout the scene. Since the approach proposed in Norman et al. (2020) produced very large individual under-segmentation errors from the last column of the table, it can be suggested that our proposed approach produced the best overall segment quality.

	Assessment Metrics				
Segmentation Assessment Methods	**QR**	**AFI**	**US**	**OS**	**RMSE**
Vamsee et al., (2018)	0.307	-0.145	0.312	0.295	0.304
Norman et al., (2020)	0.483	0.001	0.017	0.017	0.017
Elsebaei, et al., (2024)	0.150	-0.070	0.100	0.060	0.082
The proposed method	0.036	-0.011	0.073	0.072	0.073

Table 8. Segmentation error assessment comparison between our proposed strategy and some of the existing state of the art methods

5. Conclusions

Object-based image analysis (OBIA) critically depends on the quality of image segmentation. However, selecting optimal parameters to achieve meaningful segmentation results remains a significant challenge. This study introduces an unsupervised system designed to identify effective combinations of colour factor weight and scale parameter that yield meaningful segments in urban remote sensing imagery. The proposed approach offers an alternative to the strategies outlined by Vamsee et al. (2018), Norman et al. (2024), and Elsebaie et al. (2024). The system consists of three main modules. The first module, grounded in the concept of standard deviation, calculates image variance independently of segment area, addressing a key limitation of commonly used image variance modules that are sensitive to segment size. The later module is prone to any over- or under-segmentation that may affect the correct outlines of the segmented object. The second module is a robust spatial autocorrelation system that combines the formulation of the image standard deviation and the well-known Moran index formulations. The third module identifies the best parameter combination through a global score curve that defines the best parameter combinations as the peak points of the curve. The validation of the newly proposed segmentation parameter selection system was performed through intense testing with a colour aerial photograph covering an urban area made of medium-sized and large building units. Medium-sized building units were better segmented when a large colour weight value is associated with a medium-scale parameter threshold. The scale parameter of 50 required a colour weight of about 0.7 to achieve segments that are internally homogeneous and distinct from their respective neighbours. In contrast, it was found that a large-scale parameter would achieve good segment quality only if associated with a medium weight of colour factor. The scale parameter of 110 required the colour weight to be calibrated to 0.5 in order to achieve success. The proposed segmentation parameter selection system enables us to identify two optimal segmentation levels that characterize the various objects within the scene. Extensions of this work would include testing the strategy on very high-resolution satellite imagery and more complex urban landscapes that would include informal settlements. The integration of the proposed strategy with other types of remote sensing datasets such as radar or Lidar imagery could also be investigated in future studies.

References

Blanche, T., 2010. Object based image analysis for remote sensing. *ISPRS journal of photogrammetry and remote sensing*, *65*(1), pp.2-16.

Chen, G., Wing, Q., Hay, G.J. and He, Y., 2018. Geographic object-based image analysis (GEOBIA): Emerging trends and future opportunities. *Geoscience & Remote Sensing*, *55*(2), pp.159-182.

Cai, Z., Hu, Q., Zhang, X., Yang, J., Wei, H., He, Z., Song, Q., Wang, C., Yin, G. and Xu, B., 2022. An adaptive image segmentation method with automatic selection of optimal scale for extracting cropland parcels in smallholder farming systems. *Remote Sensing*, *14*(13), p.3067.

Dracut, L., Chili, O., Esan, C. and Teide, D., 2014. Automated parameterization for multi-scale image segmentation on multiple layers. *ISPRS Journal of photogrammetry and Remote Sensing*, *88*, pp.119-127.

El-nagger, A.M., 2018. Determination of optimum segmentation parameter values for extracting building from remote sensing images. *Alexandria engineering journal*, *57*(4), pp.3089-3097.

Elsebaei, M.A.E., M El-Naggar, A., KHz Abdel-maggid, R., A Elsebaei, M. and M Ayaan, S., 2024. Identification of optimal segmentation parameters for extracting buildings from remote sensing images with different resolutions. Benha *Journal of Applied Sciences*, 9(5), pp.1-11.

Ez-zahouani, B., EL Kharki, O., Kanga Idé, S. and Zouiten, M., 2023. Determination of Segmentation Parameters for Object-Based Remote Sensing Image Analysis from Conventional to Recent Approaches: A Review. *International Journal of Geoinformatics*, *19*(1).

Georganos, S., Grippa, T., Lennert, M., Vanhuysse, S., Johnson, B.A. and Wolff, E., 2018. Scale matters: Spatially partitioned unsupervised segmentation parameter optimization for large and heterogeneous satellite images. *Remote Sensing*, *10*(9), p.1440.

Grippa, T., Georganos, S., Lennert, M., Vanhuysse, S. and Wolff, E., 2017, October. A local segmentation parameter optimization approach for mapping heterogeneous urban environments using VHR imagery. In *Remote Sensing Technologies and Applications in Urban Environments II* (Vol. 10431, pp. 79-97). SPIE.

Grybas, H., Melendy, L. and Congalton, R.G., 2017. A comparison of unsupervised segmentation parameter optimization approaches using moderate-and high-resolution imagery. *Geoscience & Remote Sensing*, *54*(4), pp.515-533.

Hu, X. and Xu, H., 2018. A new remote sensing index for assessing the spatial heterogeneity in urban ecological quality: A case from Fuzhou City, China. *Ecological Indicators*, *89*, pp.11-21.

Ikokou, G.B.; Malale, K.M., 2024. Unsupervised Image Segmentation Parameters Evaluation for Urban Land Use/Land Cover Applications. *Geomatics*, 4, 149-172.

Ikokou, G.B., Smit, J., 2021. Optimal segmentation parameters prediction using a orthogonal decomposition approach for geographical object based classification of urban areas. *The Egyptian Journal of Remote Sensing and Space Science*, 24(3), 501-507.

Johnson, B.A., Bragais, M., Endo, I., Magcale-Macandog, D.B. and Macandog, P.B.M., 2015. Image segmentation parameter optimization considering within-and between-segment heterogeneity at multiple scale levels: Test case for mapping residential areas using landsat imagery. *ISPRS International Journal of Geo-Information*, *4*(4), pp.2292-2305.

Kavzoglu, T. and Yildiz, M., 2014. Parameter-based performance analysis of object-based image analysis using aerial and Quikbird-2 images. *ISPRS Annals of the Photogrammetry, Remote Sensing and Spatial Information Sciences*, *2*, pp.31-37.

Lu, H., Liu, C., Li, N., Fu, X. and Li, L., 2021. Optimal segmentation scale selection and evaluation of cultivated land objects based on high-resolution remote sensing images with spectral and texture features. *Environmental Science and Pollution Research*, *28*, pp.27067-27083.

Mohan Vamsee, A., Kamala, P., Martha, T.R., Vinod Kumar, K., Jai Sankar, G. and Amminedu, E., 2018. A tool assessing optimal multi-scale image segmentation. Journal of the *Indian Society of Remote Sensing*, 46, pp.31-41.

Norman, M., Mohd Shafri, H.Z., Idrees, M.O., Mansor, S. and Yusuf, B., 2020. Spatio-statistical optimization of image segmentation process for building footprint extraction using very high-resolution WorldView 3 satellite data. *Geocarto International*, *35*(10), pp.1124-1147.

Ozturk, M.Y. and Colkesen, I., 2024. A novel hybrid methodology integrating pixel-and object-based techniques for mapping land use and land cover from high-resolution satellite data. *International Journal of Remote Sensing*, *45*(16), pp.5640-5678.

Tonbul, H. and Kavzoglu, T., 2020. A spectral band-based comparison of unsupervised segmentation evaluation methods for image segmentation parameter optimization. *International Journal of Environment and Geoinformatics*, *7*(2), pp.132-139.

Wang, Y., Qi, Q., Liu, Y., Jiang, L. and Wang, J., 2019. Unsupervised segmentation parameter selection using the local spatial statistics for remote sensing image segmentation. *International Journal of Applied Earth Observation and Geoinformation*, *81*, pp.98-109.

Yang, L., Mansaray, L.R., Huang, J. and Wang, L., 2019. Optimal segmentation scale parameter, feature subset and classification algorithm for geographic object-based crop recognition using multisource satellite imagery. *Remote Sensing*, *11*(5), p.514.

Zhu, H., Cai, L., Liu, H. and Huang, W., 2016. Information extraction of high-resolution remote sensing images based on the calculation of optimal segmentation parameters. *PloS one*, *11*(6), p. e0158585.